Inertial sensing with classical atomic beams

Markus K. Oberthaler, Stefan Bernet, Ernst M. Rasel, Jörg Schmiedmayer, and Anton Zeilinger
Institut für Experimentalphysik, Universität Innsbruck, Technikerstrasse 25 A-6020 Innsbruck, Austria
(Received 6 March 1996)

A different approach to high-precision measurement of rotation, acceleration, and gravitation is presented. Our Moiré deflectometer is based on geometric propagation of an atomic (or molecular) beam through a set of three identical gratings. Accelerated movements of the gratings with respect to the atomic beam result in a change of the total transmitted intensity. The device is nondispersive, i.e., atoms with a broad energy distribution and without collimation can be used. Furthermore, rotational and linear (gravitational) acceleration can easily be distinguished and measured simultaneously. In a certain sense the Moiré deflectometer represents the classical analog to a quantum-mechanical matter-wave interferometer. Experimental results on a test system demonstrate that its sensitivity to rotation and gravitation is already in the range of commercially used inertial sensors. It can be increased straightforwardly by orders of magnitude. [S1050-2947(96)04010-3]

PACS number(s): 03.75.Dg, 06.30.Gv

I. INTRODUCTION

High sensitivity inertial sensors are of interest both in fundamental and in applied physics. Gyroscopes and accelerometers are commercially used for navigation in aeronautics, on satellites, in submarines, and for geological applications. Ultrahigh sensitivity devices might be employed for testing fundamentals of general relativity theory like the Lense-Thirring effect or the equivalence principle [1–3]. There are many approaches for the design of ultrahigh sensitivity accelerometers and gyroscopes using atom interferometers [4–7]. Inertial effects have been studied extensively both in optical and in neutron interferometry [8–11]. For the detection of rotation, interferometers make use of the Sagnac effect where a fringe shift due to a rotational motion of the whole system results, which is proportional to the area enclosed by the interferometer paths.

In contrast, our approach consists of a purely classical device, based on the geometric imaging properties of a series of identical periodic structures, the Moiré effect. In its original form, the Moiré effect describes how the overlapping of fine periodic structures creates a beating with a much larger spatial period. This is used for magnifying small spatial shifts of a grating with respect to a reference grating, in analogy with interferometric measurements, where small phase shifts are resolved by coherent superposition with a reference wave. In the Moiré deflectometer, the Moiré principle is implemented by using a sequence of three identical gratings, which are passed successively by an atomic beam. Behind the first two gratings the atoms are distributed in a shadow image forming sets of fringes, very similar to an atom interferometer, at various distances from the second grating. These fringes can be measured using the Moiré effect by scanning the third grating in a direction transverse to the atomic beam. A similar three-grating setup was discussed theoretically by Dubetsky and Berman [12] with emphasis on atomic lithography applications.

If such a device is in accelerated motion a fringe shift of the shadow image results. We show, that this fringe shift is identical to the one obtained in a corresponding three-grating Mach-Zehnder interferometer, as already realized [13–16].

In the following, we will outline the principles of inertial measurements with the Moiré deflectometer and with interferometers. Afterwards we will describe our experimental setup and present our results of measurements of rotation and gravitation, and in the outlook we discuss future applications and possible improvements of the Moiré deflectometer.

II. THE MOIRÉ DEFLECTOMETER

A schematic sketch of our Moiré-imaging setup is shown in Fig. 1. It consists of three material gratings which are equally spaced and aligned parallel to each other. An atomic beam passes the three gratings successively. The first two gratings select propagation directions of an originally diverging atomic beam in such a way, that an atomic density modulation is created at the position of the third grating. This modulation corresponds to an image of the collimation gratings. Such an imaging is a characteristic self-focusing feature

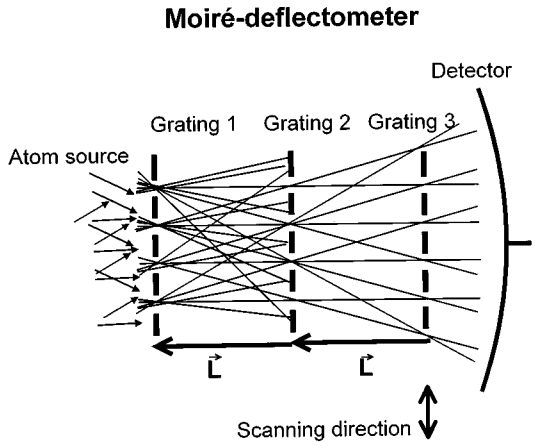

FIG. 1. Principle of a Moiré deflectometer. The first two identical gratings collimate the originally undirected atoms into various directions. After a distance L corresponding to the distance between the first two gratings, an image of the collimation gratings is formed. At this position, a third identical probe grating is placed. Its translation along the indicated direction leads to a periodic modulation of the transmitted intensity.

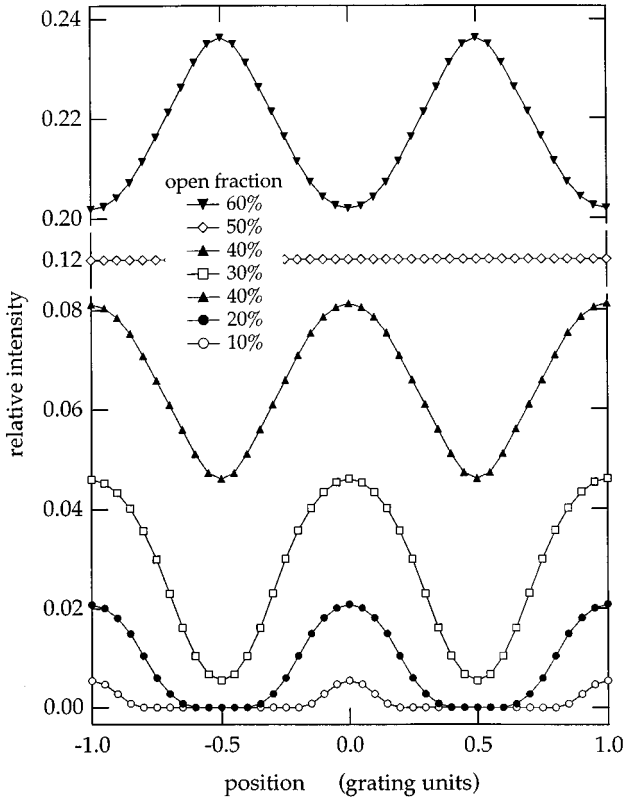

FIG. 2. Fringe patterns, as obtained by translating the third grating, calculated for various open fractions f_{open} of the gratings. For $f_{\text{open}}<25\%$ the fringe pattern shows distinct peaks at the position of the shadow image. For $25\%<f_{\text{open}}<50\%$ the fringes show an increasing constant background, and at $f_{\text{open}}=50\%$ they vanish completely. For $f_{\text{open}}>50\%$ the fringes reappear but are shifted by half a grating period (π fringe shift).

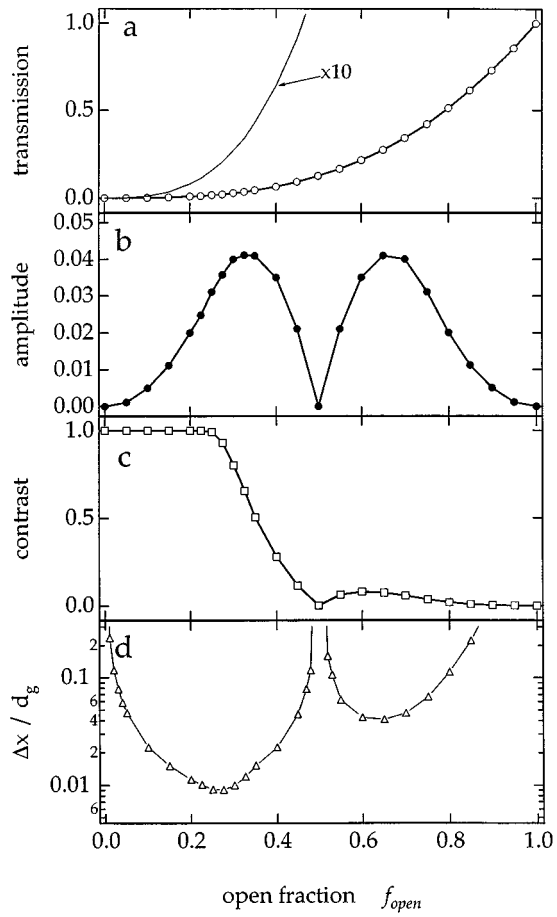

FIG. 3. Characteristic parameters of the Moiré deflectometer and their dependence on the open fraction f_{open} of the gratings. The top graph (a) shows the total transmission through the three-grating setup, (b) shows the amplitude of the obtained fringe pattern, and (c) the resulting contrast. The lowest graph (d) displays the minimal deflection in units of the grating period d_g that can be detected if 10 000 atoms impinge on the Moiré deflectometer.

of any two-grating setup. It can be explained by drawing the geometric paths of an undirected beam through the grating slits, as shown in Fig. 1. The illustration shows, that in the plane of the third grating all atomic trajectories which are selected by the slits of the first two gratings are intersecting and forming a periodic atomic density modulation with the gratings periodicity. Due to geometric ray optics such an imaging appears periodically at those distances from the second grating which correspond to integer multiples of the distance between the first two gratings.

The atomic density modulation is detected using the Moiré effect to resolve its fine periodic structure by superposing it with the third grating of the same spatial frequency. By scanning this grating in the direction of its grating vector (indicated in Fig. 1) the total atomic intensity transmitted through the apparatus oscillates with the grating period (see Fig. 2).

Looking at the classical shadow pattern of a two grating arrangement one sees that for a high fringe contrast at the position of the third grating the beams have to be narrower than the grating period. Calculations assuming a geometric propagation of an uncollimated beam through a set of three identical thin gratings show (Fig. 3) that the contrast C of the Moiré fringes equals 100% for an open fraction of less than 25% and decreases monotonically in the range of 25% to 50%. Simultaneously, the transmission of the grating set increases. Best resolution to a small fringe shift $\Delta\varphi$ is obtained at an open fraction of approximately 30% [Fig. 3(d)] which we use in our experimental setup. In this case, the fringe contrast is $C=80\%$ and the mean transmission of the three-grating set is 2.7% of the original atomic beam intensity.

Our Moiré imaging device is very well suited for measuring deflections by a classical force F. The fringe shift $\Delta\varphi$ is related to the classical deflection Δx by $\Delta\varphi=2\pi\Delta x/d_g$, where d_g is the period of the grating. The high resolution of our device arises from the small spatial structure of the grating (period d_g) and the big available atomic flux through the large area gratings. It may be noted, that the easiest way to use the same principle would be to substitute the three gratings with three single slits. Simply counting the possible trajectories one sees that the transmission of the three-grating setup is increased by the factor $N^2/2$, as compared to a three-slit setup with the same resolution, where N is the number of slits in each grating.

III. PRINCIPLES OF INERTIAL MEASUREMENTS

The inertial sensitivity of atomic beam devices originates from the fact, that a freely propagating atomic beam defines

a local inertial system. Thus any apparent deviation from linear flight in the reference frame of an observer has to be attributed to an accelerated motion of his system, or to a force acting on the atomic beam, for example, gravitation.

Specifically, the inertial sensitivity of our Moiré deflectometer arises because the image formed by the atoms is located at a predetermined location in inertial space, which appears shifted if the device accelerates during the time the atoms are in transit. In this simple context the fringe shift in our Moiré deflectometer can be thought of as arising from the transverse shift of the fringe pattern with respect to the moving gratings.

The following calculations will be performed in the laboratory system. Consider atoms with a velocity v, spending the time $\tau=L/v$ between each pair of gratings, which are separated by the distance L. The atoms pass the three gratings at the times $t=-2\tau$, $-\tau$, and 0, respectively. The ith grating is located at the position $\vec{z}_i(t)$. For reasons of simplicity, we assume a constant atomic velocity and disregard second-order corrections due to the directional anisotropy of the atomic beam. These approximations are exactly justified in the case of time-dependent atom detection selecting only atoms which spend equal times within the setup. In the case of CW measurements a small second-order correction for the derived fringe shift of the order $\Delta\Phi/\Phi=(d/L)^2$ (where d is the size of a grating) has to be considered. We chose the origin of our coordinate system at the position of the third grating at the atoms arrival time $t=0$: $\vec{z}_3(0)=(0,0,0)$ which means that $\vec{z}_1(0)=2\vec{L}$ and $\vec{z}_2(0)=\vec{L}$. The final displacement $\vec{X}$ of the atomic fringe pattern $\vec{z}_3^A(0)$ with respect to the position of the third grating $\vec{z}_3(0)$ is

$$\vec{X}=\vec{z}_3^A(0)-\vec{z}_3(0)=2\vec{z}_2(-\tau)-\vec{z}_1(-2\tau). \tag{1}$$

The corresponding fringe shift (expressed in radians) is

$$\Phi_M=\vec{k}_g\cdot[2\vec{z}_2(-\tau)-\vec{z}_1(-2\tau)], \tag{2}$$

where $\vec{k}_g$ is the reciprocal grating vector with $|\vec{k}_g|=2\pi/d_g$, and d_g is the period of the gratings. Just for clarity, it should be emphasized that this phase describes only the relative position of the fringes of the atomic distribution in the plane of the third grating, and should not be confused with the matter-wave phase.

Applied to the case of a linear acceleration of magnitude a of the whole setup in a direction parallel to the grating vector, where $z_i(t)=1/2at^2$, we get $X=-a\tau^2$ and

$$\Phi_{\rm acc}=-k_g a\tau^2=-k_g a\,\frac{L^2}{v^2}. \tag{3}$$

Due to the equivalence principle the same result is obtained for a Moiré apparatus resting in a gravitational field which acts in the opposite direction as the acceleration in Eq. (3) ($a=-g$).

Simultaneously, in the case of a rotation of the whole system with an angular rate $\vec{\Omega}$ around a center located in the deflectometer plane at the distance $\vec{l}$ from the position of the third grating (the origin of our coordinate system), we get $\vec{z}_1(t)=2\vec{L}+\vec{\Omega}\times(2\vec{L}-\vec{l})t$ and $\vec{z}_2(t)=\vec{L}+\vec{\Omega}\times(\vec{L}-\vec{l})t$ which yields

$$\Phi_{\rm rot}=2k_g\Omega_\perp v\tau^2=2k_g\Omega_\perp\,\frac{L^2}{v}, \tag{4}$$

where $\Omega_\perp$ is the component of the angular velocity perpendicular to the Moiré-deflectometer plane. Note, that the same result is obtained by substituting the Coriolis acceleration $\vec{a}=2\vec{v}\times\vec{\Omega}$ into Eq. (3).

It is an important feature of our setup that the phase shifts in the cases of rotation and acceleration sensing have different functional dependences on the particle velocity v. This can be used to measure in one experiment both rotational motion and linear acceleration (or gravitation) simultaneously. The simplest way to achieve this would be to do the experiment with two different atomic velocities and use the system of equations Eq. (3) and Eq. (4) to calculate the rotation and acceleration velocities.

Another important problem which can be eliminated using the velocity dispersion results from the fact, that the Moiré setup might actually bend under the action of an inertial force. This could imply that the measured displacement of the Moiré fringes can be in part just caused by the distortions of the apparatus. It is very crucial to note that Eq. (3) and Eq. (4) permit correction for this effect by performing a measurement at least at three different particle velocities. This follows from the fact, that with a phase offset Φ_0 the measured Moiré-fringe phase can be expressed as

$$\Phi=-k_g\,\frac{L^2}{v^2}\,a+2k_g\,\frac{L^2}{v}\,\Omega_\perp+\Phi_0. \tag{5}$$

This equation contains the three unknowns a, $\Omega_\perp$, and Φ_0. Realizing that Φ_0 is independent of the atom velocity v, we can really determine all three unknown parameters by measuring the total fringe shift Φ at least at three different velocities v. It should be noted, that the derivation of the fringe shift considers only the simplified case of a one-dimensional problem. For arbitrary motion sensing in three dimensions a measurement of six independent fringe shifts is necessary in order to determine the altogether six components of $\vec{\Omega}$ and $\vec{a}$. This can be performed, for example, by employing three Moiré deflectometers oriented perpendicular to each other, with counterpropagating atomic beams. In this case the derivation of the phase shift has to be extended and becomes more complicated than in our simple one-dimensional approach.

IV. COMPARISON OF THE MOIRÉ-DEFLECTOMETER WITH AN ATOM INTERFEROMETER

As already mentioned, the Moiré deflectometer represents the classical analog for a Mach-Zehnder type three-grating interferometer. The major design difference is, that the grating period of the Moiré setup is large enough to make diffraction negligible. This is fulfilled, if the first-order diffraction angle of the atoms is so small, that the diffracted beams are displaced by much less than one grating period on their way between two successive gratings. The corresponding relation between the grating period d_g, the de Broglie wavelength of the atoms λ_{dB}, and the grating separation L is

$$d_g\gg\sqrt{\lambda_{dB}L}. \tag{6}$$

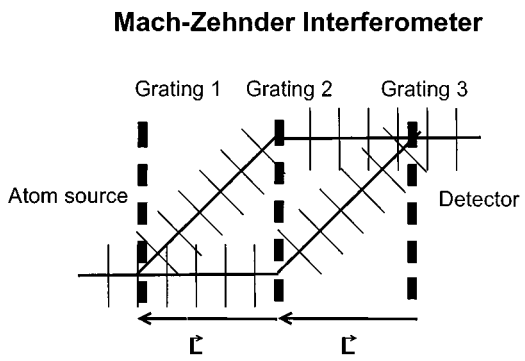

FIG. 4. The Mach-Zehnder interferometer splits a plane wave at the first grating into two waves, which are redirected by the second grating and superpose at the position of the third grating. The period and phase of the interference pattern at the position of the third grating coincide exactly with the atomic density modulation at the corresponding position in the Moiré deflectometer. Scanning of the third grating yields the same periodic transmission oscillations as in the Moiré case.

Note, that the characteristic separation $L=d_g^2/\lambda_{dB}$ corresponds to the Talbot length [18,19] which distinguishes near-field from far-field diffraction. For a more detailed analysis considering also single-slit diffraction effects and deviations from the plane-wave approach we refer the reader to [17]. A similar three-grating setup explicitly designed to work in the Talbot regime has been demonstrated in [14] where also its potential applicability as a rotation sensor is mentioned.

The principle of a Mach-Zehnder type interferometer is to split the incoming atomic beam at the first grating into two waves which are redirected by the second grating to overlap at the position of the third grating (Fig. 4). There they form an interference pattern with the same period and position as the density modulation obtained in the Moiré imaging case. Just as there, scanning of the third grating over the modulation pattern yields periodic transmission oscillations.

The similar behavior of a Mach-Zehnder interferometer and our Moiré apparatus is related to the fact that both employ the same three-grating geometry and, thus, both exhibit white-light fringes. In an inertial system all interference fringes formed by any wave vectors with arbitrary absolute values and directions of incidence coincide. Therefore, even for a Mach-Zehnder interferometer neither spatial nor temporal coherence of the incoming de Broglie waves is required. Thus the Moiré sensor can be viewed as the correspondence limit of the Mach-Zehnder interferometer, which is achieved if the mass of the atoms and, hence, the de Broglie frequency becomes infinitely large.

We discussed the inertial sensitivity of the Moiré setup extensively in the last section. The same arguments apply also to the inertial sensitivity of a three-grating interferometer. However, as a comparison we will give here a different viewpoint for the phase shifts in an interferometer. Due to the beam splitting and recombining at the diffraction gratings an interferometer encloses a particular area within its two paths. The inertial sensitivity of an interferometer for accelerated motions can be seen as arising from the fact, that the de Broglie waves experience different Doppler shifts on their alternative paths from the first to the last grating [20]. In the laboratory system, the additional frequency $\Delta\omega$ of a de Broglie wave due to a grating moving with velocity $\vec{v}_g$ is $\Delta\omega=\pm\vec{k}_g\cdot\vec{v}_g$, for diffraction into the orders ±1, respectively. If such a frequency offset is applied during a time interval t_g, then a corresponding phase shift $\Phi_D=\pm\int_0^{t_g}\vec{k}_g\cdot\vec{v}_g(t)dt$ is picked up by the de Broglie wave as compared to another wave which experiences no Doppler shift. In an interferometer the total phase difference between the two paths is the fringe shift Φ_I of the accelerated setup with respect to the motionless case. In the Mach-Zehnder geometry shown in Fig. 4 this is given by

$$\Phi_I=\int_{-2\tau}^{0}\vec{k}_g\cdot\vec{v}_{g1}(t)dt-2\int_{-\tau}^{0}\vec{k}_g\cdot\vec{v}_{g2}(t)dt, \qquad (7)$$

where τ is the transit time of the atom between two adjacent gratings, and $\vec{v}_{g1}=\dot{\vec{z}}_1$, $\vec{v}_{g2}=\dot{\vec{z}}_2$, are the velocities of the first and second gratings, respectively. By using these relations and performing the integration we get

$$\Phi_I=\vec{k}_g\cdot[2\vec{z}_2(-\tau)-\vec{z}_1(-2\tau)]. \qquad (8)$$

This result, which is valid for all types of (nonrelativistic) movements, is identical to the fringe shift Φ_M of the Moiré deflectometer as obtained in the preceding section [Eq. (2)]. Therefore the results for the special cases of linear acceleration and rotation as calculated before [Eq. (3) and Eq. (4)] for the Moiré case can be used also for the interferometer.

Note, that this reveals a surprising correspondence between a quasistatic ''snapshot'' description [21], where the grating positions are only regarded at fixed moments in time, and a ''dynamic'' Doppler-effect description, where the velocity of the gratings during the whole transit time is important, because the corresponding phase shift has to be integrated.

In an interferometer, the particles are described as matter waves by assigning a wave vector $k_{\mathrm{atom}}=m_a v/\hbar$ to an atom with mass m_a. Therefore, using Eq. (3) one gets

$$\Phi_{\mathrm{rot}}=k_g 2v\tau^2\Omega=k_g\frac{2m_aL^2}{m_a v}\Omega=\frac{2m_a}{\hbar}\vec{A}\cdot\vec{\Omega}, \qquad (9)$$

where $A=L^2(k_g/k_{\mathrm{atom}})$ is the area enclosed by the paths of the interferometer. This phase shift due to rotation is the well-known Sagnac effect. Note, that this equation, which is usually derived by quantum-mechanical analysis, is now obtained just by ''artificially'' substituting $p=\hbar k$ into the purely classical result obtained for the Moiré deflectometer.

In the same way, originating from Eq. (4), the phase shift due to a uniform acceleration of an interferometer can be calculated as

$$\Phi_{\mathrm{acc}}=-\vec{k}_g\cdot\vec{a}\tau^2=-\vec{k}_g\cdot\vec{a}\left(\frac{L}{v}\right)^2=-\frac{m^2}{\hbar^2k_{\mathrm{atom}}}a_sA, \qquad (10)$$

where a_s is the magnitude of the acceleration component parallel to the grating vector k_g. We have again related the transit time to the area of the interferometer. These results are valid for any kinds of two-path interferometers [22].

Comparing the Moiré deflectometer with the Mach-Zehnder interferometer it is striking that only geometric properties determine the resolution of the Moiré

deflectometer—its dimensions and the velocity of the atoms. On the other hand, the interferometric phase shift [Eq. (9) and Eq. (10)] includes a material property, the mass of the atoms. The mass dependence can be canceled out due to the proportionality between the atomic mass, the wave vector of the atoms, and the area enclosed by the interferometer paths. This argument remains even valid for grating interferometers with light. Therefore, according to Eq. (3), atomic devices are much more sensitive than light interferometer with the same physical dimensions, due to the lower atomic velocity.

A frequently heard argument is, that the area enclosed by the interferometer determines its resolution for inertial measurements. However, the area enclosed by a certain interferometer can be varied almost arbitrarily, without any change in resolution by using particles with a different mass. This is the basic reason why a Moiré setup without any enclosed area yields the same resolution as a corresponding interferometer.

The above similarities between the classical apparatus and a quantum-mechanical interferometer can also be understood by investigating the behavior of the fringe shift as compared to the classical deflection of the atomic beam.

A change in the propagation direction of an atomic beam can be attributed classically to a force, $\vec{F}$, acting on the atoms, or quantum mechanically to a transverse phase gradient acquired by the atomic de Broglie wave. $\vec{F}$ can be viewed as stemming from a potential gradient $\vec{F}=-\vec{\nabla}U$. Such a potential gradient acting at a propagating matter wave will lead to a phase gradient of the matter wave, which is exactly the one necessary in order to account for the deflection of the beam. This is because the transverse phase gradient leads to a tilting of the wave front and therefore to a change of the propagation direction of the atomic wave. The resulting fringe shift is identical to the classical deflection of the atoms due to the force $\vec{F}=-\vec{\nabla}U$. The role of the third grating in both cases is to measure the shift of the atomic distribution with a ruler. Thus, when comparing the sensitivities of the two devices, one realizes that while the ruler can be much finer in the case of an atom interferometer, the intensity used can be higher in the case of a Moiré deflectometer, and it is a question of the specific experimental conditions which of the two apparata is more sensitive in a certain context.

We finally remark that the shift of the envelope of the atomic distribution is identical to the fringe shift in all situations which can be explained by simple classical mechanics [23]. This is not the case if one detects a phase shift in just one interferometer arm, or if one studies topological or geometrical phases. In this case one has to use the quantum-mechanical properties of the interferometer for a description of the experiment.

V. BANDWIDTH AND SENSITIVITY

An experimental parameter which has to be considered is the velocity distribution of the atomic beam. In contrast to the static case, both a Moiré deflectometer and a Mach-Zehnder interferometer in accelerated motion are dispersive. While on the one hand, as pointed out above, the dispersion can be used to separate angular motion from acceleration and for a zero calibration of the deflectometer, it also limits the measurement bandwidth in continuous mode applications. The wavelength dependence of the fringe shift can lead to two effects. Firstly, it implies a reduction of the intensity modulation, i.e., of the observed contrast, and secondly, it can lead to a measurement error in the sense that the mean measured fringe shift is not necessarily the fringe shift of the mean beam velocity.

In the case of a rotation measurement, the fringe shift $\Delta\Phi_{\mathrm{rot}}$ due to a velocity change of Δv can be derived from Eq. (4) as $\Delta\Phi_{\mathrm{rot}}=(-)\Phi_{\mathrm{rot}}\Delta v/v$. A velocity distribution which is symmetric around the central velocity yields a fringe distribution, which is also symmetric around the fringe position corresponding to the peak velocity. In that case only a reduction of the contrast results. For sinusoidal fringes (which are an adequate approximation for the real shape of our fringes at our grating's open fraction 0.3, as can be seen in Fig. 2) the contrast reduction factor f is calculated as

$$f=2-\left[\frac{1}{\Delta\Phi_{\mathrm{rot}}}\int_{-\Delta\Phi_{\mathrm{rot}}/2}^{\Delta\Phi_{\mathrm{rot}}/2}\cos(x)\,dx\right]^{-1}=2-\frac{\Delta\Phi_{\mathrm{rot}}/2}{\sin(\Delta\Phi_{\mathrm{rot}}/2)}. \tag{11}$$

To obtain the actual contrast of the atomic intensity modulation, the theoretical contrast $C=(I_{\max}-I_{\min})/(I_{\max}+I_{\min})$ for the mean beam velocity has to be multiplied with the contrast reduction factor f which is always smaller than 1. The contrast vanishes if $f=0$, which happens for the first time at $\Delta\Phi_{\mathrm{rot}}=1.21\pi$. In the case of our atom source with $v=750$ m/s, $\Delta v_{FWHM}=400$ m/s, $L=0.27$ m, and $k_g=2\pi/d_g=6.3\times10^5\ \mathrm{m}^{-1}$, the maximum rotation rate which can be measured is therefore limited by the velocity distribution of our source to about 50 mrad/s. On the other hand, for the earth's rotation rate of 7.3×10^{-5} rad/s, the contrast is only reduced by a factor of 10^{-6}. All rotation frequencies investigated experimentally in the present paper yield a negligible contrast reduction by less than 10^{-5}.

We now estimate the resolution of a Moiré setup and of an interferometer. We define the resolutions for rotations R_{rot} and accelerations R_{acc} as the infinitesimal fringe shifts which occur as a function of an infinitesimal change in rotation frequency or in acceleration, respectively

$$R_{\mathrm{rot}}=\left|\frac{\partial\Phi_{\mathrm{rot}}}{\partial\Omega}\right|=2k_g\frac{L^2}{v},$$

$$R_{\mathrm{acc}}=\left|\frac{\partial\Phi_{\mathrm{acc}}}{\partial a}\right|=k_g\frac{L^2}{v^2}. \tag{12}$$

These resolutions are just features of the apparatus and therefore independent of the intensity used. In order to have a quantitative measure of the accuracy achievable within a given measurement time one has to include the statistics and therefore the flux of the registered atoms. For simplicity, we assume a Poissonian distribution of the detection events which results in a signal-to-noise ratio which is proportional to $C\sqrt{N}$, where C is the fringe contrast ($C\leqslant1$) and N is the number of counts in a given set of data.

The minimal resolvable angular velocity and acceleration ($\Omega_{\min}$) is therefore inversely proportional to the square root of the measurement time t, where the proportionality factor S is the sensitivity

$$\Omega_{\min} = S/\sqrt{t}. \tag{13}$$

With n being the average count rate per unit time the sensitivities are

$$S_{\mathrm{rot}} = \frac{1}{R_{\mathrm{rot}} C \sqrt{n}},$$

$$S_{\mathrm{acc}} = \frac{1}{R_{\mathrm{acc}} C \sqrt{n}}. \tag{14}$$

The sensitivities may be viewed as the minimal angular rotation frequency or acceleration measurable in unit time. Note, that due to our definition a smaller value of the sensitivity corresponds to a more accurate device and vice versa. In order to optimize the sensitivity, both high count rate and high fringe contrast are necessary. As shown before (Fig. 2, and Fig. 3) the compromise for best sensitivity is obtained at an open fraction of approximately 30% which we use in our experimental setup. In this case, the theoretical fringe contrast is $C=80\%$, and the mean transmission through the three gratings corresponds to 2.7% of the original atomic beam intensity.

Inspection of Eq. (12) and Eq. (14) shows that for a given size of the apparatus L and a given atomic velocity v, the sensitivities are proportional to the grating period and inversely proportional to the square root of the count rate. Comparing thus the performance of a Moiré deflectometer with that of an atom interferometer, we realize that while the advantage of the latter is its finer grating period. On the other hand, the advantage of the Moiré deflectometer is that much higher intensities can be used, because no atomic beam collimation is necessary in order to obtain a high fringe contrast, as in the case of an atom interferometer [24]. It is a question of the experimental details which of the two factors is more advantageous in a given situation.

VI. THE EXPERIMENTAL SETUP

The experimental setup consists of an atom source, the actual Moiré-grating arrangement and a channeltron detector. In the source, Argon gas at a pressure of 10 mbar is excited by an electric discharge and leaves the source in its metastable $^1S_5$ state which can be detected by the channeltron. The lifetime of this state (>10 s) is much longer than the traveling time of the atoms (3 ms) through the apparatus. The discharge burns from a cathode within the source to a skimmer at ground potential. The source can be operated in continuous mode or in pulsed mode. In continuous mode the metastable Argon atoms leave the source with an average velocity of 750 m/s. The velocity distribution exhibits a single broad peak with a width of 400 m/s [full width at half maximum (FWHM)]. In pulsed mode a double peak structure appears in the velocity distribution, with two maxima at velocities of 600 m/s and 920 m/s. The FWHM of the two peaks are 140 m/s and 260 m/s, respectively. Behind the skimmer the gas jet enters the vacuum chamber with the Moiré setup which is kept at a pressure of 10^{-7} mbar.

The Moiré setup consists of three identical, fine machined gold gratings with a grating period of 10 μm and a slit width of 3 μm within each period. The size of the gold gratings is (3 mm$\times$3 mm). The three gratings are mounted on an optical bench with a separation of 27 cm. They are aligned parallel to each other (within 300 μrad tolerance) and perpendicular to the atomic beam. The last grating is mounted on a flexure translation stage and can be shifted by a few grating periods in a direction perpendicular to the grating bars with sub-μm accuracy using a piezo transducer. If the third grating is moved linearly, a periodic modulation of its transmission is observed due to the geometric reasons explained above,—the Moiré-fringe structure. Behind the last grating, the transmitted atoms are detected by a channeltron detector, and counted by a multichannel counter card. The contrast of the Moiré fringes depends on the precision of the parallel alignment of the gratings, and the equality of their spacings. We achieve typically 70% contrast, which is close to the maximal theoretical value of 80%, expected for our gratings with an open fraction of 3/10, as explained above. In our experiment, we measure the position of these fringes as a function of accelerated motions of the Moiré setup.

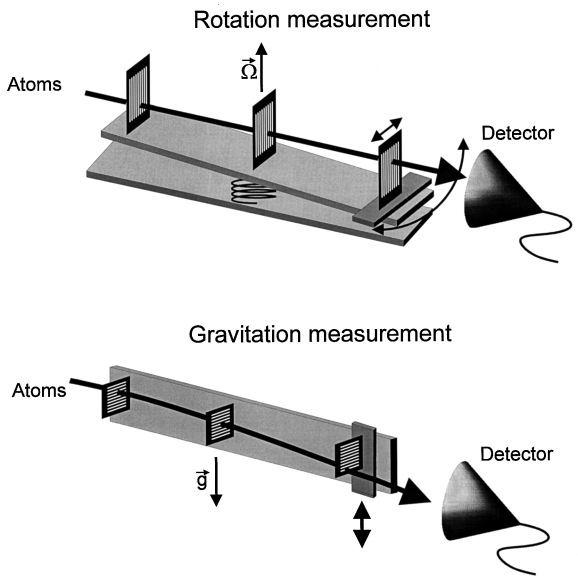

FIG. 5. Experimental setup for measuring rotation (a) and gravitation (b). For measuring the fringe shift due to the Coriolis force (a), the Moiré setup is mounted on an optical bench which oscillates with a small amplitude around its center. The transmission is measured as a function of the instantaneous angular velocity of the setup. For measuring the Earth's gravitation (b), the optical bench is turned by 90°. Due to the parabolic trajectory of the atoms a velocity dependent fringe shift results when scanning the third grating. By measuring this fringe shift as a function of the time-of-flight of the atoms, the value of g is obtained by extrapolation to zero flight time.

VII. ROTATION MEASUREMENTS

For our rotation measurements we operated the atom source in continuous mode. The gratings were mounted with their grating lines oriented vertically as shown in Fig. 5(a). Instead of rotating the whole vacuum system continuously with a constant angular rate we measured the fringe shift caused by oscillatory rotational motion of the three-grating setup alone. In contrast to typical applications where the

Moiré deflectometer would be used to sense an accelerated motion the atom source was not moving. Both setups correspond to the same physical situation because of the directional isotropy of the atomic beam. If the atom source is also rotating, just another fraction of the isotropic atomic beam passes the deflectometer with no effect on the observable fringe shift.

In the experiment the whole optical bench with the three gratings was mounted on a torsion spring located at the center of the bench resulting in oscillations around a vertical axis (rotation vector parallel to gravity). Resonant vibrations of the whole bench were excited by an oscillating piezo crystal tipping periodically at the bench. Mainly, two resonance frequencies of the bench at 10 Hz and 577 Hz were used, with typical oscillation amplitudes of 5 μm and 100 nm, respectively. For the 10 Hz vibration, the whole bench could be assumed to rotate with an almost constant angular frequency during the traveling time (0.75 ms) of an atom through the 54 cm long Moiré setup. For the 577 Hz oscillation, a correction of 35% to the measured sensitivity had to be taken into consideration, due to the fact that the bench changed its angular velocity during the passage of an atom. The instantaneous angular acceleration of the optical bench was measured with two mechanical acceleration sensors, mounted at equal distances from the rotation axis at both ends of the optical bench. They were oriented such that they were sensitive to accelerations along directions parallel to the grating vectors. A second independent measurement of the motional parameters was performed with an optical interferometer, measuring the vibration amplitudes and relative velocities of the two outer edges of the optical bench. From both measurements the vibration amplitude, angular velocity and angular acceleration could be obtained independently. The results of the acceleration sensors and the interferometer agreed within 5% uncertainty.

During an experimental run the whole optical bench was oscillating harmonically. Simultaneously, the third grating, which was mounted on a translation stage, was scanned periodically over two-grating periods with a sawtooth scanning function at a low repetition frequency of typically 0.25 Hz. This scan was phase locked to the faster bench vibrations by a trigger pulse which started the translation stage scan always at a fixed phase of the bench vibrations. The same trigger pulse started the multichannel counter, which registered the transmitted atoms as a function of their arrival time during one complete translation stage scanning period with a time resolution of 1 ms (40 μs) for the 10 Hz (577 Hz) vibrations. Due to the phase locking by the common trigger pulses, an integration over several translation stage scans could be performed.

Each recorded data set yielded, simultaneously, information about the phases of the Moiré fringes at many rotation frequencies within the range of the maximal rotation velocities during one bench oscillation.

Figure 6 shows an unprocessed data track which has been recorded following the procedure described above. The bench oscillation frequency and the linear scanning frequency of the translation stage have been 10.5 Hz and 0.2 Hz, respectively. For demonstrating the measurement principle, a high oscillation amplitude of 18 μm has been chosen. The low-frequency envelope of the data curve is due to the slow translation stage motion, whereas the superposed fine structure corresponds to the faster bench vibrations. For data processing it was necessary to extract all data points which belonged to the same angular velocity. This was done by sampling the data track with the exact period of the fast bench vibrations. Starting with the data points of the first bench vibration period T, the other data points belonging to the same actual rotation rate were found at distances corresponding to integer multiples of T. Two examples are plotted in the graph, indicated by squares and circles. Sinusoidal fitting curves correspond to the results which would have been obtained at a constant rotation frequency of the whole system. From the simultaneously recorded data of the acceleration sensors and the optical interferometer, the rotation velocities belonging to these various sampled curves were determined. The phase of these curves was obtained with good accuracy by fitting a sinusoidal function to the data points, although the exact transmittance of the three gratings, consisting of a convolution of the three single transmittance functions, was not exactly harmonic.

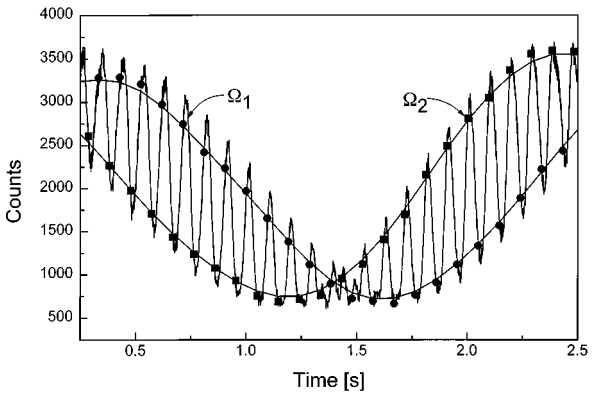

FIG. 6. Raw data of a typical rotation measurement, elapsed in 1500 seconds. The sinusoidal shaped envelope of the data results from the linear translation scan of the third grating. The fast oscillations are due to the bench vibrations with a frequency of 10.5 Hz and an amplitude of 18 μm. The data is processed by sampling the data track with the bench oscillation frequency, starting successively at the data points within the first vibration period. Two examples (squares and circles) are indicated for two rotation rates Ω_1 and Ω_2. Sinusoidal fits through these sampling points correspond to transmission data for a fixed angular velocity. The phase of these fringes is proportional to the instantaneous rotation velocity of the bench.

A plot of the fringe shift as a function of the rotation frequency is sketched in Fig. 7. It shows a linear behavior as expected from Eq. (4). The experimental resolution is derived from the slope of this plot as $130\times 2\pi$ rad/Hz. The deviation from its theoretical value $122\times 2\pi$ rad/Hz calculated according to Eq. (12) is mainly due to our poor knowledge of the atomic beam velocity during dc operation of the source. With this experimental resolution the effect of the earth's rotation ($\Omega_{\text{earth}}=7.3\times 10^{-5}$ Hz/2π) consists in a fringe shift of 9.5 mrad.

The inset of Fig. 7 shows the results of a more accurate measurement performed in the rotation frequency range indicated by the rectangle. In this experiment the resonant 577 Hz bench vibration was chosen. Due to its higher vibration frequency this implied a much smaller vibration amplitude in

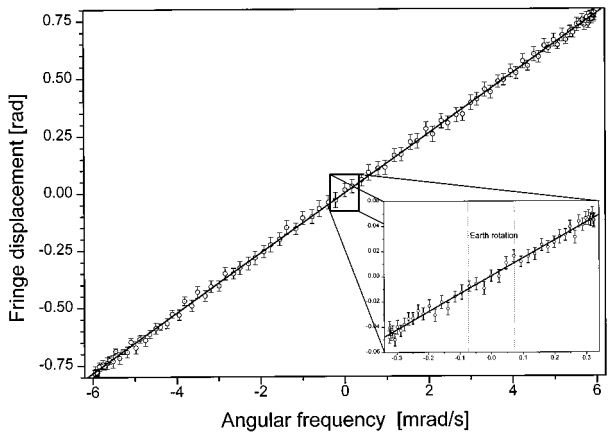

FIG. 7. Phases of the sinusoidal fringes obtained from the data of Fig. 6, as a function of the angular velocity. A linear behavior is observed according to Eq. (4). The slope yields the experimental sensitivity of our setup: $130\times 2\pi$ rad/Hz. The inset shows the results of a finer measurement with a resolution better than earth's rotation.

a fixed measurement interval. In the experiment the vibration amplitude was reduced to 20 nm which is only 2×10^{-3} of the 10 μm grating period. The result shows, that rotation frequencies of the order of the earth's rotation rate (indicated by the dotted lines) are resolved. The error bars correspond to the standard deviation of the fringe shifts, fitted with sinusoidal functions. In this experiment it has to be considered that during the measurement period of 24 minutes, 44 independent phase measurements have been performed using the method described above. Thus the experimental time needed for one phase value was 30 s. From the corresponding standard deviation of each rotation measurement we can estimate that for resolving a rotation frequency with a standard deviation of the order of the earth's rotation, we need 13 s measurement time. This corresponds to a sensitivity of 2.6×10^{-4} rad $\sqrt{s}$. A theoretical estimation according to Eq. (14) with our mean count rate of 18 500 counts/s and our experimental contrast of 70% yields a theoretically possible sensitivity of 8.1×10^{-5} rad $\sqrt{s}$, which is by a factor 3 better than our experimental value. We assume that the discrepancy is due to nonlinearities of our flexure stage scans, small phase drifts of the bench oscillations during the repetitive measurements, and to the fact that our experimental data is fitted with sinusoidal functions, which is only an approximation to the real shape of the transmission signal.

VIII. GRAVITATION MEASUREMENTS

A complete measurement of the inertial motion of a system includes also a measurement of the linear acceleration. Due to the equivalence principle of relativity theory acceleration is indistinguishable from the action of gravity. For simplicity, we therefore decided to determine the gravitational action on our Moiré fringes.

In order to measure the value of the local gravity g the whole optical bench in the Moiré setup was turned by 90° around its longitudinal axis and the bench oscillation mounts were removed. Now the atomic beam passed the three gratings whose bars were oriented horizontally [Fig. 5(b)]. The parabolic trajectory of the atomic beam yielded a fringe shift with respect to the vertical alignment used before. The third grating was still scanned parallel to its grating vector, which corresponded now to the vertical direction. An estimation of the resolution of this setup for acceleration measurements [Eq. (12)] yields 0.08 rad/(ms^{-2}). Thus the effect of the earth's gravitational field consists in an easily observable fringe shift of 0.8 rad or 13% of the grating period. Nevertheless, it is hard to separate this from mechanical stress effects which might occur when turning the optical bench. Therefore, we used for the measurement of g the velocity dispersion of the fringe position. From Eq. (3) it is obvious that for gravitational measurements the fringe shift is a parabolic function of the atoms time of flight. Extrapolation of the fringe position to infinite atomic velocity gives the hypothetical fringe position without gravity. This yields an absolute calibration without requiring a reference measurement at zero gravity or zero acceleration.

Technically, we performed time resolved measurements with a pulsed atom source with a broad velocity spectrum. We used the fact that in a special mode of pulsed operation our Argon gas source generated two well separated velocity groups with peaks at 600 and 920 m/s, respectively. They were probably produced by different types of gas discharges burning during a short (5 μs) pulse. By adjusting other source parameters (gas pressure, distance between cathode and skimmer, discharge voltage), it was possible to get almost equal count rates for both velocity peaks. A typical time-of-flight spectrum of the atoms is shown in Fig. 9 (dotted line).

During a measurement cycle, the atom source was pulsed with a repetition frequency of 6 ms and a pulse duration of 5 μs. The pulsing was obtained by switching the electric discharge voltage on and off. This resulted in a pulsed production of the metastable atoms. The time of flight of the fast (920 m/s) atoms in the 2.10 m long vacuum chamber was approximately 2.3 ms, whereas the slow atoms (600 m/s) traveled for 3.3 ms. The pulse duration of 5 μs was negligible with respect to the FWHM of the arrival times (0.65 and 0.80 ms, respectively). The third grating was again scanned slowly (scanning frequency: 4 Hz) with a sawtooth function over approximately one grating period. The start of each scan was synchronized with the emission of an atomic pulse by a common trigger signal. The same trigger signal started the counting of the detected atoms into successive time channels with a time resolution of 30 μs, for the duration of one translation stage scan. Repetitive measurement cycles could be integrated due to the synchronization by the common trigger signals.

A typical chart of raw data is shown in Fig. 8. The sinusoidal envelope is due to the linear translation stage scan, which was obtained as the rising edge of an actually performed sawtooth scan. Within this envelope the repetition of the pulses with a period of 6 ms yields the fine structure. Magnification of the data in the inset of Fig. 8 shows, that its fine structure is composed of successively arriving pulses. Each double peak structure belongs to one single gas discharge. To obtain fringes which correspond to constant atomic velocities the data was processed as before. Successively starting with the individual data points of the first pulse the other data points belonging to the same atomic

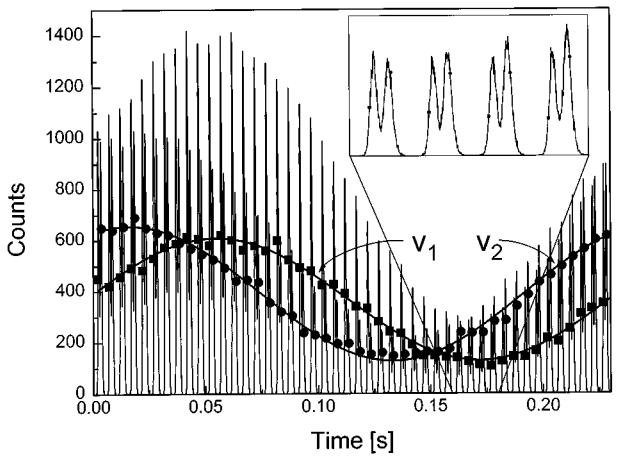

FIG. 8. Measurement of local gravitational acceleration using a time-of-flight measurement with the setup of Fig. 5(b). The whole data was acquired in 100 min. The sinusoidal envelope of the data is again due to the linear scan of the third grating. Within this envelope a series of repetitive time-of-flight spectra is recorded (see magnification in the inset). Each time-of-flight spectrum consists of a double peaked pulse produced by our atom source. The pulses are emitted during a 5 μs gas discharge with a repetition period of 6 ms. The time of flight of the two peak centers of each pulse is 2.3 and 3.3 ms, respectively. Sampling of the data track with the pulse repetition period of 6 ms yields sinusoidal fringes. Each of them corresponds to a flexure stage scan at a fixed atomic velocity. Two examples for sampled data points at two-different velocities v_1 and v_2 are plotted, together with harmonic fit curves. The phases of these fringes depend quadratically on the corresponding atomic velocities.

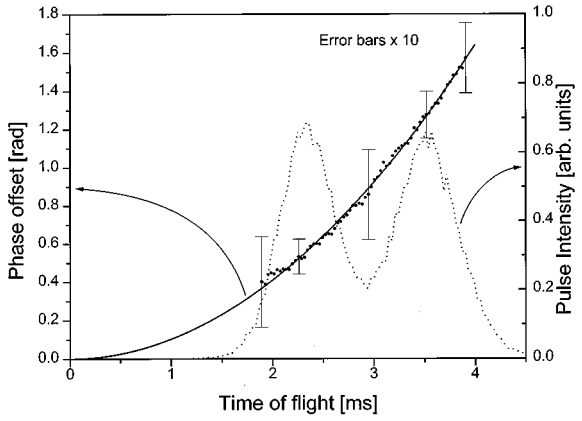

FIG. 9. Fitted phases of the transmission fringes of Fig. 8 as a function of their corresponding times of flight. According to Eq. (3) a parabolic dependence is obtained. From the curvature the value for $g=(9.86\pm0.07)$ ms^{-2} is calculated. The dashed line shows the time-of-flight spectrum of a single pulse. Comparison of the error bars (magnified by a factor 10 in the plot) with the time-of-flight spectrum shows, that the size of the errors depends reciprocally on the square root of the intensity of the atoms at the corresponding velocity.

velocity (but another position of the third grating) were found at integer multiples of the pulse repetition period. Examples are shown in Fig. 8 for two different starting points within the first pulse period (squares and circles). They show fringes which are periodic with the translation stage frequency. The phases of these fringes depend on the corresponding atomic velocities. Data points obtained for the same atomic speed are again fitted with sinusoidal functions (also indicated in Fig. 8), and the fringe phases are plotted as a function of the atomic velocities in Fig. 9. The error bars correspond to the standard deviations obtained by the phase fits. The same figure shows a time-of-flight spectrum (dotted line) of one atomic pulse in order to demonstrate the accessible measurement range. In agreement with Eq. (3) a parabolic dependence of the fringe position on the flight time is observed

$$\frac{\partial^2\Phi_{acc}}{\partial t^2}=\frac{2gk_gL^2}{L_z^2}, \tag{15}$$

where $L_z=2.10$ m is the path length from the atom source to the detector, $L=0.27$ m is the distance between successive Moiré gratings, $k_g=6.28\times10^5$ m^{-1} is the magnitude of the reciprocal grating vector, and t is the flight time.

From the curvature of the parabolic function the value of g is determined as $g=(9.86\pm0.07)$ ms^{-2}. The absolute accuracy of this value is only limited by our knowledge of the geometric constants in our setup, whereas the relative accuracy, which corresponds to the size of the error bars in Fig. 9, depends on the number of integrated counts. The total time elapsed in this experiment was 105 minutes yielding an experimentally achieved sensitivity of 0.56 g s$^{1/2}$.

This means, e.g., that, after calibration of our setup, the value of g can be obtained in 24 h with a relative accuracy of 2×10^{-4}. Much better sensitivities due to higher count rates are possible, if the setup is calibrated by a reference signal (e.g., a light beam) and thus can be used with a dc atomic beam, instead of our short pulses.

IX. DISCUSSION

For an evaluation of the practical potentials of the Moiré deflectometer it has to be compared to actual ''state-of-the-art'' gyroscopes (Fig. 10) and acceleration sensors.

The experimentally achieved rotation sensitivity of the Moiré deflectometer is actually 3.6 $\Omega_e s^{1/2}$, where $\Omega_e=7.3\times10^{-5}$ rad/s is the earth's rotation rate. This means that rotational velocity changes of the order of the earth's rotation rate can be detected in approximately 10 s.

Other approaches which have been investigated experimentally are rotation sensors with atom interferometers [25], electron interferometers [26], a Ramsey-type atom interferometer with Ca atoms [6], and neutron interferometers [9]. The best resolution is reached by the neutron interferometer due to the diffraction of slow neutrons at very fine gratings consisting of the atomic lattices of a Si crystal. Nevertheless, the sensitivity of this interferometer is only in the range of our experimental result with the Moiré deflectometer because of the low count rates of the neutron beam experiments. Almost the same high resolution and an improved sensitivity due to a Na-atom source which is by a factor 10^7 brighter than our Ar source is obtained with a Mach-Zehnder atom interferometer using material gratings with 200 μm period [25].

Due to low count rates the sensitivity of the Ramsey-type Ca-atom interferometer is more than 3 orders of magnitude

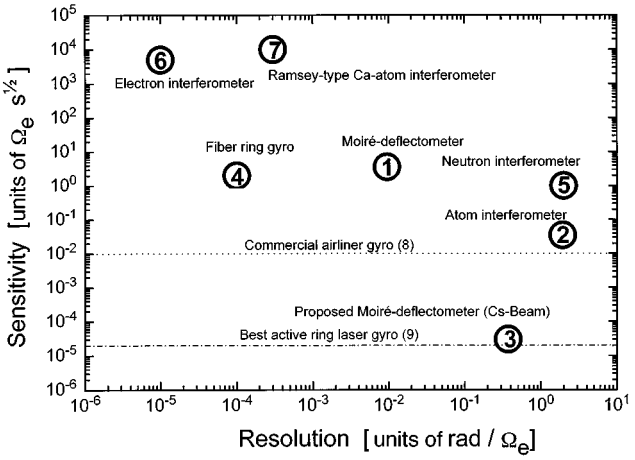

FIG. 10. Comparison of the resolutions and sensitivities of different rotation sensors. The resolution is plotted in units of the fringe shift (in rad) created by the angular velocity of the earth's rotation. The sensitivity corresponds to the minimal resolvable rotation rate (scaled in units of the earth's rotation) within an integration time of 1 s. Best performance of rotation sensors corresponds to high resolution and low sensitivity. Point 1 shows our actual experimental result. Similar sensitivities are reached by a passive ring laser system (point 4, [27]), and a Mach-Zehnder type neutron interferometer (point 5, [9]). A Na-atom interferometer (point 2, [25]) has almost the same high resolution as the neutron interferometer and a better sensitivity, due to the huge intensity of the atom source. An electron interferometer (point 6, [26]) has a lower resolution and a worse sensitivity by three orders of magnitude. A Ramsey-type atom interferometer (point 7, [6]) with a neutral Ca atomic beam has a sensitivity which is worse by four orders of magnitude. In actual commercial airliners sensitivities in the range of $10^{-2}\ \Omega_e s^{1/2}$ are required (dotted line 8, [3]). This is surpassed by two orders of magnitude with a straightforwardly optimized Moiré deflectometer as proposed in text (point 3). Better sensitivities in the range of $2\times10^{-5}\ \Omega_e s^{1/2}$ are only obtained with the highly sophisticated large active ring laser gyro in Canterbury, New Zealand [28], the best rotation sensor reported to date (dashed-dotted line 9).

worse than the sensitivity of our Moiré setup. In contrast, the poor sensitivity of the electron interferometer does not result from poor counting statistics, but from a low resolution due to the high velocity of the electron beam.

As mentioned above, light gyroscopes with the same physical dimensions as atomic beam devices have much lower resolutions due to the different velocities of atoms and photons. But this disadvantage is usually compensated by their easier handling using fiber optics and higher intensities. By employing coils of optical fibers [27] the actual physical dimensions of the interferometer are multiplied by the number of the windings [3]. Thus passive fiber-ring gyros reach sensitivities in the range of our experimental Moiré-deflectometer result ($2\ \Omega_e\ s^{1/2}$).

More accurate rotation sensors consist of passive laser ring resonators. Commercial devices [3] reach a sensitivity of $10^{-2}\ \Omega_e\ s^{1/2}$ which is required for navigation in airliners (dotted line Fig. 10).

A highly sophisticated improvement of such a device has been built in Canterbury, New Zealand [28] (dashed-dotted line Fig. 10). It consists of a large active ring laser with 1 m^2 area which is located 30 m underground due to its requirements of mechanical and temperature stability. It reaches the best sensitivity reported up to date, of $2\times10^{-5}\ \Omega_e\ s^{1/2}$.

For a comparison with the Moiré deflectometer it has to be considered that we use a nonoptimized test device with large potential for improvements. First, both reducing the period of the Moiré fringes and the velocity of the atomic beam results in a linear improvement of the resolution, according to Eq. (12). Increasing the length of the setup results even in a quadratic improvement, although it has to be considered that a decrease of the number of transmitted atoms might result, depending on the divergence of the atomic beam. A considerable improvement of the sensitivity can be obtained by enlarging the intensity of the atomic beam [Eq. (14)]. Cesium atom sources as used in standard atomic clocks have intensities (10^{10} atoms/s) which are by a factor 5×10^5 larger than our actual source. Simultaneously, their thermal atomic velocity is reduced by a factor of 3, due to the higher mass of the Cs atoms. Both effects together improve the sensitivity by a factor of 2×10^3. It should be noted, that the geometric parameters for the proposed Moiré deflectometer are chosen such that they are close to the constraints given by inequality Eq. (6), which separates the classical particle regime from the wave-mechanical Talbot regime. However, since the inertial sensitivity remains also preserved in the transition from particle mechanics to the wave-mechanical case (see Sec. IV above), a too rigid borderline between the two cases is not necessary with respect to potential geometrical improvements. Summarizing, an optimized but still reasonably straightforward Moiré deflectometer with a Cs atom source might employ gratings with 10 μm period, separated by 1 m. Such a device would reach a resolution of 0.37 rad/Ω_e, which is four orders of magnitude better than the commercially used fiber-coil systems. Its sensitivity of $3\times10^{-5}\ \Omega_e\ s^{1/2}$ would be comparable with the best reported rotation sensor in Canterbury, and significantly better than commercial ring laser gyros.

The advantage of atomic beam devices with respect to photons is even increased in applications as acceleration or gravitation sensors, due to the fact, that the resolution is a quadratic function of the reciprocal velocity [Eq. (12)]. Interferometric approaches for measuring the gravitation constant have been already demonstrated with neutron interferometers [9], which have, as in their applications as rotation sensors, the advantage of a high resolution, but the disadvantage of low count rates.

Our experimentally achieved sensitivity of 0.56 $g\ s^{1/2}$ is still rather poor, due to the pulsed operation of our Argon source resulting in a low intensity of the atomic beam. Nevertheless, the results can be used to estimate the performance of the optimized Moiré deflectometer with the Cesium source described above. Using it in continuous mode for acceleration or gravitation measurements, a theoretical sensitivity of $1.2\times10^{-7}\ g\ s^{1/2}$ can be reached (where $g=9.81\ ms^{-2}$ is the gravitation constant). This is orders of magnitude better than commercial mechanical sensors. Such an accuracy would, for example, be sufficient for detecting the gravitational effect of a 10t mass at a distance of 2.5 m in 100 s. Furthermore, by using time resolved measurements an absolute calibration standard is inherently available, as demonstrated in the experiment.

Practical applications of the Moiré inertial sensor have the

major advantage of allowing measurements of the complete motional state of a system using a single principle. According to Chasles' theorem [29] the knowledge of rotation and acceleration is sufficient for tracing the complete motion of any system. With counterpropagating atomic beams, rotation- and acceleration-induced fringe shifts can be separated due to their different signs, with both being measured simultaneously. Another possibility is to use the different functional dependence of the fringe offset on the velocity in the cases of rotation (linear dependence) and acceleration (quadratic dependence). Measuring the fringe shift at three different atomic beam velocities allows us, in principle, to determine the rotation and acceleration of the system simultaneously, and includes an absolute calibration of the fringe offset corresponding to an inertial system. Practically, such a measurement might be performed simultaneously using an atomic beam with a broad velocity distribution and velocity-sensitive detection.

A nice detail in practical applications would also be to use the Moiré effect in its original form: as a magnification of fine periodic structures by superposition with structures of almost equal period. Hereby, the last grating would have a slightly different period than the others, or it would be rotated slightly. In this case the fringe shift would translate into a periodic intensity pattern along the grating bars, which can be measured with a position sensitive detector like a microchannel array without any movements of the gratings. This will give the device a high bandwith only limited by the transit time of the atoms.

X. SUMMARY

An inertial sensor is presented which we call the Moiré deflectometer. We showed that its performance with respect to inertial effects is identical to similar systems using neutral-matter interferometry, although the principles of interferometric rotation sensors require a certain area enclosed by the beam paths. The Moiré principle which is used for detecting the atomic density modulation at the position of the third grating can be seen as a classical analogue to interferometric measurements.

Our Moiré setup with its simple design has practical applications as an inertial sensor. We demonstrated that even with our test-device rotation rates below the earth's rotation could be detected in a few seconds, and we performed a measurement of the local gravity. A better optimized but still straightforward device is proposed in the text. Its rotation resolution exceeds the best passive optical gyroscopes by orders of magnitude, and its sensitivity is in the range of the best existing optical gyro, the Canterbury ring laser. The acceleration sensitivity of such an improved Moiré deflectometer is orders of magnitude better than the best mechanical and optical devices.

A large advantage of the Moiré deflectometer is the fact that the complete motion of a system, consisting of accelerations and rotations, can be traced with a single device. Rotations and accelerations can be measured simultaneously by employing either counterpropagating beams or by utilizing the velocity dispersion of the fringe offset. This has the additional advantage of inherently including an absolute calibration of the device as we demonstrated in our determination of local gravity.

Due to these advantages—wide range applicability and high precision, which are achievable with relatively simple methods—Moiré-inertial sensors might become of interest in future fundamental research and commercial applications.

ACKNOWLEDGMENTS

This work is supported by the Austrian Fonds zur Förderung der Wissenschaftlichen Forschung (FWF), Project Nos. S06504 and P 6637-TEC. J.S. acknowledges support from the Austrian Academy of Sciences, and S.B. is supported by the HCM-programme (Contract No. ERBCHBGCT940664) of the HCM-programme the European Community. A.Z. acknowledges support by the U.S. National Science Foundation Grant No. PHY 92-13964.

[1] J. Anandan, Phys. Rev. D **15**, 1448 (1977).
[2] M. P. Haugan, M. O. Scully, and K. Just, Phys. Lett. **77A**, 88 (1989).
[3] W. W. Chow, J. Gea-Banacloche, L. M. Pedrotti, V. E. Sanders, W. Schleich, and M. O. Scully, Rev. Mod. Phys. **57**, 61 (1985).
[4] J. F. Clauser, Physica B **151**, 262 (1988).
[5] R. Anderson, H. R. Bilger, and G. E. Stedman, Am. J. Phys. **62**, 975 (1994).
[6] F. Riehle, Th. Kisters, A. Witte, J. Helmcke, and Ch. Bordé, Phys. Rev. Lett. **67**, 177 (1991).
[7] M. Kasevich and S. Chu, Phys. Rev. Lett. **67**, 181 (1991).
[8] R. Colella, A. W. Overhauser, and S. A. Werner, Phys. Rev. Lett. **34** (23), 1472 (1975).
[9] J. L. Staudenmann, S. A. Werner, R. Colella, and A. W. Overhauser, Phys. Rev. A **21**, 1419 (1979).
[10] S. A. Werner, H. Kaiser, M. Arif, and R. Clothier, Physica B **151**, 22 (1988).
[11] D. K. Atwood, M. A. Horne, C. G. Shull, and J. Arthur, Phys. Rev. Lett. **52**, 1673 (1984).
[12] B. Dubetsky and P. R. Berman, Phys. Rev. A **50**, 4057 (1994).
[13] D. W. Keith, C. R. Ekstrom, Q. A. Turchette, and D. E. Pritchard, Phys. Rev. Lett. **66**, 2693 (1991).
[14] J. F. Clauser and S. Li, Phys. Rev. A **49**, R2213 (1994).
[15] E. M. Rasel, M. K. Oberthaler, H. Batelaan, J. Schmiedmayer, and A. Zeilinger, Phys. Rev. Lett. **75**, 2633 (1995).
[16] D. M. Giltner, R. W. McGowan, and S. A. Lee, Phys. Rev. Lett. **75**, 2638 (1995).
[17] J. F. Clauser and M. W. Reinsch, Appl. Phys. B **54**, 380 (1992).
[18] H. F. Talbot, Philos. Mag. **9**, 401 (1836).
[19] M. S. Chapman, C. R. Ekstrom, T. D. Hammond, J. Schmiedmayer, B. E. Tannian, S. Wehinger, and D. E. Pritchard, Phys. Rev. A **51**, R14 (1995).
[20] M. Dresden and C. N. Yang, Phys. Rev. D **20**, 1847 (1979).

[21] D. M. Greenberger and A. W. Overhauser, Rev. Mod. Phys. **51**, 43 (1979).
[22] S. F. Jacobs and R. Zanoni, Am. J. Phys. **50**, 659 (1982).
[23] A. Zeilinger, in *Fundamental Aspects of Quantum Theory*, edited by V. Gorini and A. Frigerio (Plenum, New York, 1986).
[24] Q. A. Turchette, D. E. Pritchard, and D. W. Keith, J. Opt. Soc. Am. A **9**, 1601 (1992).
[25] A. Lenef *et al.* (unpublished).
[26] M. Nicklaus, Ph.D. thesis, Tübingen (Germany), 1989.
[27] R. A. Bergh, H. C. Lefevre, and H. J. Shaw, Opt. Lett. **6**, 198 (1981).
[28] G. E. Stedman, H. R. Bilger, Li Ziyuan, M. P. Poulton, C. H. Rowe, I. Vetharaniam, and P. V. Wells, Aust. J. Phys. **46**, 87 (1993).
[29] See, for example, J. B. Marion, *Classical Dynamics of Particles and Systems*, 2nd ed. (Academic, New York, 1970).